Desalination and Water Treatment
www.deswater.com
doi: 10.1080/19443994.2014.936515

56 (2015) 425–434
October

Taylor & Francis
Taylor & Francis Group

Fabrication of Ag/halloysite nanotubes/Fe_3O_4 nanocatalyst and their catalytic performance in 4-nitrophenol reduction

Mengying Gan[a,b], Yongqiang Huang[a,*], Yunlei Zhang[a,b], Jianming Pan[b], Weidong Shi[b], Yongsheng Yan[b]

[a]*School of Environment, Jiangsu University, Zhenjiang 212013, China, Tel. +86 051188790930; Fax: +86 051188790955; emails: yqhuang@ujs.edu.cn, jsdx2011@126.com (Y. Huang)*
[b]*School of Chemistry and Chemical Engineering, Jiangsu University, Zhenjiang 212013, China, Tel. +86 051188791800; email: zhenjiangpjm@126.com (J. Pan)*

Received 10 October 2013; Accepted 12 June 2014

ABSTRACT

Ag/halloysite nanotubes/Fe_3O_4 (Ag/HNTs/Fe_3O_4) nanocatalyst was synthesized in our work. The structure of the as-prepared composite catalyst was that Fe_3O_4 nanoparticles with the size of 5.0–8.0 nm were loaded in the internal hollow lumen of HNTs and Ag nanoparticles with a mean diameter of 20 nm were randomly deposited on the external surface of HNTs/Fe_3O_4. The resultant Ag/HNTs/Fe_3O_4 exhibited satisfied catalytic activity (with conversion of 100% in 38 min) to the reduction of 4-nitrophenol (4-NP) with sodium borohydride. The catalytic activity was markedly enhanced when the catalysts concentration was increased (the rate constant was gradually increased from 0.40 to $20.18 \times 10^{-3}\,s^{-1}$). Also, the advantage of the obtained magnetic composite catalyst in terms of their fast separation and simple reuse was identified through five successive catalytic and separation process cycles. It could be concluded that Ag/HNTs/Fe_3O_4 showed satisfied catalytic activity, recoverability, and reusability, which showed great potential for practical application for water treatment.

Keywords: 4-Nitrophenol (4-NP); Ag nanocatalyst; Catalytic activity; Magnetic separation; Halloysite nanotubes (HNTs)

1. Introduction

Nitroaromatic compounds (NACs) are toxic and biorefractory, used extensively as raw materials and intermediates in the production of explosives, pharmaceuticals, pesticides, pigments, dyes, wood preservatives, and rubber chemicals [1]. 4-Nitrophenol (4-NP) is an important member of the NAC family due to its high chemical stability, water solubility, persistence, and toxicity to the life forms. Hence, 4-NP has been listed as the priority pollutant by the United States Environmental Protection Agency (USEPA) [2]. 4-NP also has been proved to release into the soil as a result of the hydrolysis of the organophosphate pesticides, such as parathion and methyl parathion, and herbicides, such as dinoseb and dinitrocresol [3–6], especially in the developing world where there is widespread use of these pesticides. Consequently, the groundwater resources were contaminated though the 4-NP permeated in the soil. Additional, their removal from surface water and groundwater is hindered due to their high stability and solubility in water as well

*Corresponding author.

as their resistance to traditional water purification methods [7].

Recently, it was reported that silver nanoparticles can be used as a catalyst for the reduction of 4-NP due to their distinctive physicochemical properties. The reduction of 4-NP to 4-aminophenol (4-AP) with an excess amount of $NaBH_4$ has often been used as a model reaction to test the catalytic performance of Ag nanoparticles. Moreover, 4-AP has important applications as an analgesic and anti-pyretic drug, such as acetanilide, phenacetin, paracetamol, and so on [8]. Additional, 4-AP is also widely used as a corrosion inhibitor in paints, a dyeing agent, an anticorrosion-lubricating agent, and a photographic developer in fuels for two-cycle engines [9]. Bai et al. [10] and Eising et al. [11] used metal Ag nanoparticles as catalyst, which have proved that it have relative high catalytic activity in reducing 4-NP. Up to now, there were many routes to synthesize silver nanoparticles with various shapes for desired properties, such as wet chemical reduction in aqueous solutions [12–14], microemulsion method [15,16], hydrothermal method, and micro-emulsion method [17]. Li [18] and co-workers have prepared Ag nanoparticles by the reduction of silver nitrate with sodium borohydride. Lu [19] and co-workers have synthesized Ag particles by UV irradiation. However, silver nanoparticles are prone to aggregation, poor in recoverability, and reusability. Therefore, it is a difficult but promising task, great endeavors should be done to address these issues.

Recently, many researchers used solid support to solve the problem of aggregation of Ag catalysts. Yu et al. [20] and Deng et al. [21] used SiO_2 as a support to avoid Ag nanoparticles aggregating. Yang and co-workers [22] adopted graphene to solve this problem, Chen et al. [23] and Dong et al. [24] deposited Ag nanoparticles on the carbon nanotube to deter it from aggregating. However, these supports seem to be expensive for practical application. Therefore, to find a low-cost and available support was urgent. Halloysite nanotubes (HNTs) were potential to be considered as the carrier of catalyst to prevent the aggregation of Ag nanoparticles. HNTs ($Al_2Si_2O_5(OH)_4H_2O$) are naturally occurring silicate nanotubes ubiquitous in soils and weathered rocks [25]. It is a two-layered clay mineral possessing hollow nanotubular structure in the submicrometer range and large specific surface area [26]. As for most natural materials, the size of HNTs varies within 1–15 μm of length and 10–150 nm of inner diameter depending on the deposits [27]. It could be considered as the substitute for Carbon nanotube. Moreover, HNTs are available in abundance in China as well as other locations around the world. What's more, HNTs have been applied in many fields where it is used as adsorbents [28]; catalyst supports [29]; electronic, biological systems, and functional materials; [30] and so on. Based on these advantages, HNTs were used as a support in this work.

Applying of magnetic separation was a good method to solve the problem of recoverability and reusability. Ding and co-workers [31] separated nano-sized magnetic catalysts well by applying the magnetic field. Dong and co-workers [32] used magnetic Fe_3O_4 core to achieve high recyclables. However, if Fe_3O_4 nanoparticles were directly used as support of noble metal, these magnetic carriers will suffer slow oxidation exposure to air. Additional, Fe_3O_4 nanoparticles were prone to aggregation if they were directly acting as support due to its small particle size (only 5.0–8.0 nm). Therefore, to slow down or prevent oxidation, Fe_3O_4 nanoparticles were loaded into the lumen of HNTs to form magnetic composites, HNTs/Fe_3O_4. Magnetic catalysts with magnetically responsive internal core and catalytic external particles have gained much attention due to their unique separable features, which makes it possible to realize controllable on–off reactions and convenient recycling of catalysts [33].

Inspired by the information mentioned above, we reported an effective method to achieve magnetic HNTs combined with the Ag particles. The catalytic activity of the Ag/HNTs/Fe_3O_4 nanoparticles was investigated by applying them as a catalyst for the reduction of 4-NP, with the assistance of sodium borohydride ($NaBH_4$). The advantages of the Ag/HNTs/Fe_3O_4 nanocatalyst in terms of their recoverability and reusability were demonstrated by many successive reduction-reaction runs, under the application of a magnetic field.

2. Experiments

2.1. Chemicals and materials

HNTs were purchased from Zhengzhou Jin yang guang Chinaware Co. Ltd., Henan, China. Ammonia, nitric acid, ethanol, glucose, and (Fe $(NO_3)_3 \cdot 9H_2O$) were all purchased from Shanghai Chemical Reagent Co. Ltd. (Shanghai, China). Silver nitrate was purchased from Shanghai fine chemical industry research institute. 4-NP was purchased from Aladdin Reagent Co. Ltd. (Shanghai, China). Deionized water was used for all experiments.

2.2. Pretreatment of HNTs

The pretreatment process of HNTs followed our previous work with a few modifications [34]. A certain amount of HNTs was dissolved in 3.8 mol L^{-1}. HNO_3

aqueous solution was magnetically stirred to wash away the impurity. Practically, 10 g HNTs was dissolved in 100 mL deionized water. Twenty five milliliter of HNO_3 was slowly added into the above solution. The mixture was then magnetically stirred and heated at 75℃ with reflux for 12 h. Then, the suspension was filtered and washed several times with distilled water in order to reach with neutral pH, and then the HNTs were dried at 50℃ overnight. After that, the product was calcined at 200℃ for 2.0 h.

2.3. Preparation of HNTs/Fe_3O_4 composites

HNTs/Fe_3O_4 composites were prepared via a simple method described as follows: 0.66 g activated HNTs and 0.33 g $Fe(NO_3)_3 \cdot 9H_2O$ were dispersed in 30 g ethanol under ultrasound bath for 60 min. Then, the mixture was evaporated to constant weight in water bath at 60℃. After soaking by propionic acid steam for 15 h at 80℃, the mixture was calcined at 265℃ in the protection of N_2 for 2.0 h. Finally, HNTs/Fe_3O_4 was obtained after washing several times with distilled water and ethanol, respectively.

2.4. Preparation of Ag/HNTs/Fe_3O_4 nanoparticles

The Ag/HNTs/Fe_3O_4 nanoparticles were synthesized by chemical-reduction method which was called silver mirror reaction [35]. Briefly, 100 mg HNTs/Fe_3O_4 was dispersed in 100 mL deionized water in a round-bottom flask and sonicated for 30 min. Analytical grade $AgNO_3$ (0.0085 g) was dissolved in 0.5 mL of deionized water in a small beaker. Then, the $AgNO_3$ solution was added into aqueous ammonia (0.1 M) in a dropwise manner under vigorous stirring until a clear colorless solution was obtained. The obtained solution was then quantitatively transferred into a 10 mL volumetric flask and was made up to 10 mL with deionized water [36] to form a $[Ag(NH_3)_2]OH$ solution. Subsequently, 10 mL of freshly prepared $[Ag(NH_3)_2]OH$ solution was added to the dispersed HNTs/Fe_3O_4 with vigorous stirring at 40℃. After 1.0 h, 10 mL glucose solution (0.0152 M) was introduced into a 10 mL syringe. Under the action of gravity, it was c automatically added dropwise into the homogeneous-dispersed mixture and stirring for another 1.0 h. After that, stirring was continued for 1.0 h. Finally, the product was collected by filtering and washing several times by water and ethanol; the reactants Ag/HNTs/Fe_3O_4 particles were dried in a vacuum oven at 80℃ for 24 h.

2.5. Material characterization

Transmission electron micrographs (TEM) were registered on a JEOL IEM-200CX) microscope operating at 200 kV and equipped with an ORIUS Gatan Camera. For the observations, the sample powders were deposited on 3 mm copper grids coated with an amorphous carbon film. Elemental mapping over the selected regions of the catalyst was conducted by EDS. The XRD patterns were obtained with a MO3XHF22 X-ray diffractometer (MAC Science, Japan) equipped with Ni-filtrated Cu K_α radiation tube over a scattering angle of 2θ range, approximately from 10° to 80° at a scanning rate of 6°min^{-1}. UV–vis diffuse reflectance spectra (UV–vis DRS) of the catalyst were obtained for the dry-pressed disk sample using specord 2450 spectrometer (Shimazu, Japan) equipped with the integrated sphere accessory for DRS, using $BaSO_4$ as the reflectance sample. Fourier transform infrared (FT-IR) spectra were recorded on a Nicolet Nexus 470 FT-IR (America thermo-electricity Company) with 2.0 cm^{-1} resolution in the range of 400–4,000 cm^{-1}, using KBr pellet. TGA was performed for powder samples (about 10 mg) using a Diamond TG/DTA Instruments (Perkin-Elmer, USA) under a nitrogen atmosphere up to 1,000℃ with a heating rate of 5.0℃/min^{-1}. Magnetic measurements were carried out using a vibrating sample magnetometer (7300, Lakeshore) under a magnetic field up to 10 kOe. Distilled water was obtained from N1T-DI deionized water equipment (Dongguan Nabaichuan Water Treatment Equipment Co. Ltd.)

2.6. Catalytic reduction of 4-NP

The catalytic reduction of 4-NP to 4-AP by $NaBH_4$ was carried out in a quartz cuvette with an optical path length of 1.0 cm and monitored using UV–vis spectroscopy at room temperature. An amount of 0.5 mL of aqueous 4-NP solution (0.12 mM) was mixed with 3.0 mL of a fresh $NaBH_4$ solution (60 mM). 0.1 mL of aqueous dispersion of Ag/HNTs/Fe_3O_4 particles was added and the mixed solution was quickly measured by UV–vis spectroscopy. After the desired time, the change of absorption was recorded *in situ* to obtain the successive information about the reaction. As the reaction proceeded, it could be observed that the solution changed gradually from yellow to colorless. The use of an excess of $NaBH_4$ was to ensure that its concentration remains essentially constant during the reaction, which allows the assumption of pseudo-first-order kinetics with respect to the 4-NP [37].

2.7. Recycling process

In the recycling study, due to real-time measurement of UV absorption, the magnetic nanoparticles were magnetically separated out of the solution after the reduction reaction was completed. The recycled magnetic catalysts were washed with ethanol three times and with deionized water three times, in a similar process. This procedure was repeated more than five times.

3. Results and discussion

3.1. TEM and EDS analysis

Microstructure of HNTs, HNTs/Fe_3O_4 and Ag/HNTs/Fe_3O_4 nanoparticles were observed by TEM and representative images were shown in Fig. 1. As shown in Fig. 1(a), the HNTs had detectable hollow tubular structure with a diameter in the range of 50–120 nm and the nanotubes were open-ended, which was a benefit for loading the nanoparticles in their nanotubes. The inner diameter of HNTs was about 20–25 nm, while the wall thickness was about 20 nm. Moreover, judging from the Fig. 1(b), the lumen was not completely filled or blocked and the well-dispersed black particles (Fe_3O_4 particles) with the small size of 5.0–8.0 nm were mainly deposited in the internal hollow lumen of the HNTs. Furthermore, from the morphology of Ag/HNTs/Fe_3O_4 (Fig. 1(c)), large amounts of Ag nanoparticles with a diameter of 20 nm were deposited on the external surface of HNTs/Fe_3O_4. The diameter of Ag particle was much smaller than that reported by Bai and co-workers [38], which was about 57 nm. Furthermore, both Fe_3O_4 and Ag nanoparticles were spherical in shape. According to the result of EDS (Fig. 1(d)), the Ag/HNTs/Fe_3O_4 particles were consisted of O, Si, Al, Fe, and Ag. The peaks of Al, Si, and O were mainly generated by HNTs and the peaks of Fe and Ag were resulted from loaded Fe_3O_4 and deposited Ag nanoparticles, respectively. It also can be seen from the Table 1, resulted from the Ag/HNTs/Fe_3O_4 particles, that the weight (%) attributed to the Fe and Ag particles were 4.71 and 7.27, respectively. All this results illustrated that

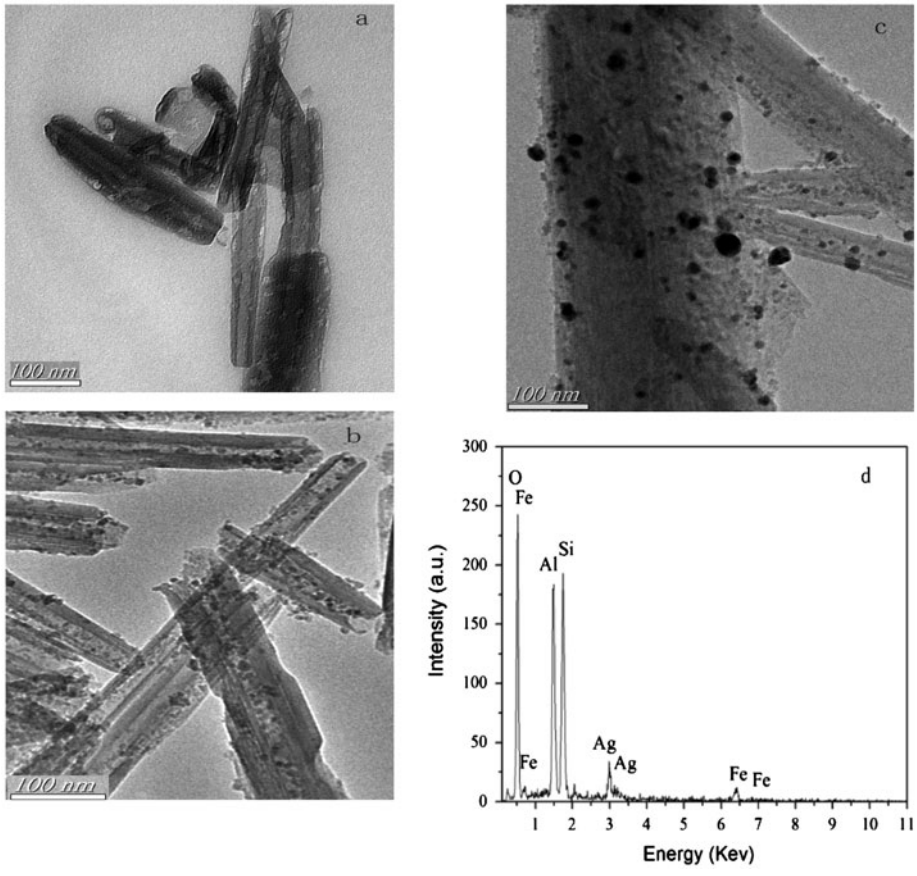

Fig. 1. TEM images of HNTs (a), HNTs/Fe_3O_4 (b), Ag/HNTs/Fe_3O_4 (c), and EDS of Ag/HNTs/Fe_3O_4 (d).

Table 1
Composition of main elements (O, Al, Si, Fe and Ag)

Element	O K	Al K	Si K	Fe K	Ag L	Total
Weight (%)	52.71	14.73	20.58	4.71	7.27	100

the Ag nanoparticles were well loaded onto the external surface of HNTs/Fe_3O_4.

3.2. XRD analysis

To verify the formation of Fe_3O_4 and Ag nanoparticles, the XRD patterns of HNTs, HNTs/Fe_3O_4, and Ag/HNTs/Fe_3O_4 are shown in Fig. 2. For the HNTs sample, the observed peaks at 20.01, 24.79, and 29.98 can be indexed to the characteristic peaks of halloysite [39]. However, the two new peaks at 35.6° and 43.2°, which can be indexed as (311) and (400) crystalline planes of Fe_3O_4 [40] (JCPDS card no. 79-0418), were both observed from HNTs/Fe_3O_4 and Ag/HNTs/Fe_3O_4 nanoparticles which suggested that Fe_3O_4 particles were formed in both the HNTs/Fe_3O_4 and Ag/HNTs/Fe_3O_4 nanoparticles. In addition, peaks at 38.1°, 44.3°, 64.4°, and 77.6° can be assigned to the reflections of (111), (200), (220), and (311) crystalline planes of cubic Ag (JCPDS cards 4-0783) [41], respectively. Moreover, no diffraction peaks corresponding to silver oxide were observed, which confirmed that only metallic Ag was formed by chemical reduction method.

3.3. UV–vis DRS analysis and FT-IR analysis

It is known that nano-sized Ag particles exhibit strong surface plasmon resonance (SPR) absorption around 400–450 nm [42]. Then, the UV–vis DRS of catalysts are presented in Fig. 3. The HNTs and HNTs/Fe_3O_4 did not show any SPR bands because there is no Ag species. The absorption peak emerged at about 420 nm after the deposition of Ag nanoparticles. The reason may be related to the formation of Ag on the surface of HNTs/Fe_3O_4.

The FT-IR spectra in the 4,000–400 cm^{-1} wave number range of (a) HNTs, (b) HNTs/Fe_3O_4, and (c) Ag/HNTs/Fe_3O_4 were also included in Fig. 4. The infrared spectrum of HNTs showed two Al_2OH stretching absorption bands at 3,694 and 3,621 cm^{-1}, each O–H being linked to two Al atoms in-plane Si–O–Si stretching (1,090 and 1,032 cm^{-1}), and a single Al_2OH bending band at 911 cm^{-1}, which were characteristic peaks of HNTs, were observed in the FT-IR spectra of the HNTs, HNTs/Fe3O4, and Ag/HNTs/Fe_3O_4 nanocomposites [25,43]. The presence of a peak at 1,385 cm^{-1} for NO_3^- vibration [44] is due to the residue of HNO_3 during the pretreatment of HNTs process. When Fe_3O_4 nanoparticles were loaded into the internal hollow of the HNTs, the height ratio between 1,090 and 1,032 cm^{-1} was decreased comparing with HNTs. Moreover, this height ratio changed into weak comparing with HNTs/Fe_3O_4 when Ag nanoparticles were deposited on the external surface of HNTs/Fe_3O_4. It could be concluded that Fe_3O_4 nanoparticles and Ag nanoparticles have an effect on Si–O–Si stretching.

3.4. TG analysis

Fig. 5 provided the TGA curves of (a) HNTs/Fe_3O_4 and (b) Ag/HNTs/Fe_3O_4. The slight weight loss below 200 ℃ was resulted from physically adsorbed water on the surface [45] of the materials and

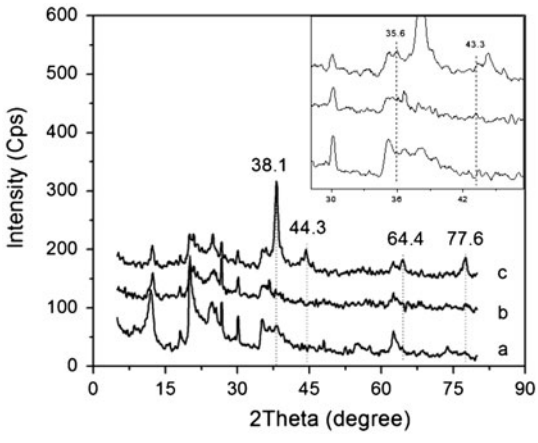

Fig. 2. XRD pattern of HNTs (a), HNTs/Fe_3O_4 (b) and Ag/HNTs/Fe_3O_4 (c).

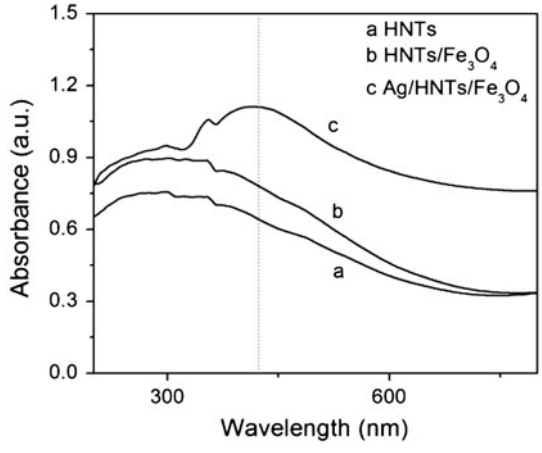

Fig. 3. UV–vis absorption spectra of HNTs (a), HNTs/Fe_3O_4 (b) and Ag/HNTs/Fe_3O_4 (c).

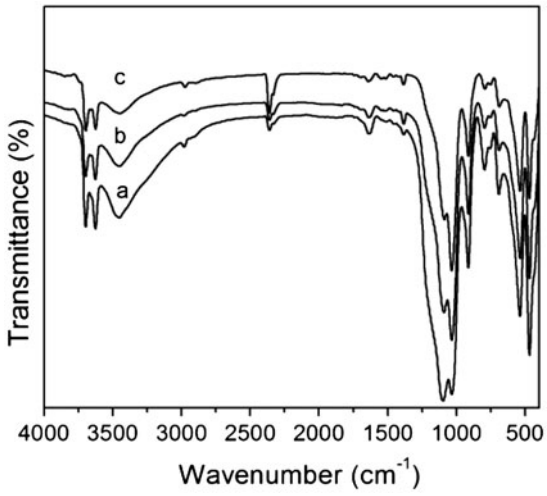

Fig. 4. FT-IR spectra of HNTs (a), HNTs/Fe_3O_4 (b) and Ag/HNTs/Fe_3O_4 (c).

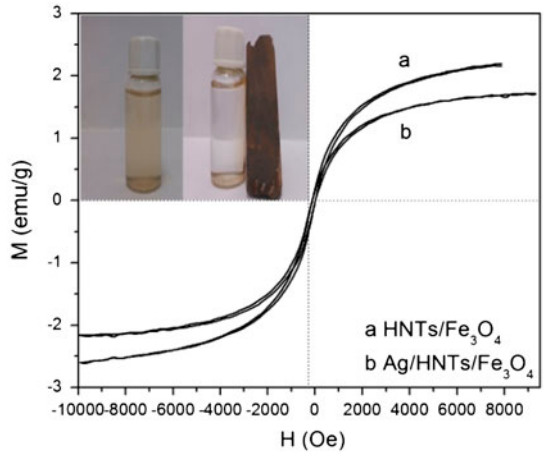

Fig. 6. Magnetic hysteresis loops of HNTs/Fe_3O_4 (a) and Ag/HNTs/Fe_3O_4 (b), and the inset is a photograph of the composites under an external magnetic field.

corresponded to 2.74% for HNTs/Fe_3O_4 and 3.94% for Ag/HNTs/Fe_3O_4, respectively. Furthermore, a sharp loss in mass at 200˚C and continued at 500˚C was observed for HNTs/Fe_3O_4 and Ag/HNTs/Fe_3O_4, possibly due to the residual water in the lumen and the dehydroxylation of structural aluminol groups [46] of the materials. However, the remaining mass of HNTs/Fe_3O_4 (89.80%) was more than that of Ag/HNTs/Fe_3O_4 (88.55%). This result may be attributed to the loss of the Fe_3O_4 nanoparticles in the preparation of Ag/HNTs /Fe_3O_4 process.

3.5. Magnetization curves

A magnetic hysteresis loop of the composite materials, as shown in Fig. 6, was recorded at room temperature. Both the remanence and coercivity were zero, suggesting that such particles were superparamagnetic. The saturation magnetization of HNTs/Fe_3O_4 nanoparticles and the Ag/HNTs/Fe_3O_4 particles was 2.19 and 1.72 emu g^{-1}, respectively. Also it can be seen that the Ag/HNTs/Fe_3O_4 particles could be well separated from the water under an external magnetic field. The two similar curves revealed that the magnetization tended to decrease from HNTs/Fe_3O_4 to Ag/HNTs/Fe_3O_4 curve as a function of the applied magnetic field. There may be two reasons for this result. One was attributed to the loss of the Fe_3O_4 nanoparticles in the preparation of Ag/HNTs/Fe_3O_4 process, which was also in accordance with the TGA result. The other one was possible that surface magnetic anisotropy was changed with the existence of Ag nanoparticles and the increased surface spins disorientation [47], consequently, decreased the magnetic moment.

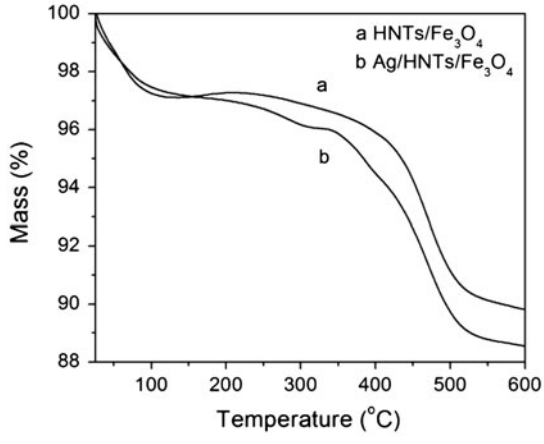

Fig. 5. TGA profiles of HNTs (a), HNTs/Fe_3O_4 (b) and Ag/HNTs/Fe_3O_4 (c).

3.6. Catalytic activity

The catalytic performance of reduced Ag/HNTs/Fe_3O_4 nanoparticles was evaluated via the catalytic reduction reaction of 4-NP by $NaBH_4$, as illustrated in Fig. 7. This reaction is particularly easy to follow because there is only one product, 4-AP, formed and the extent of reaction can be directly determined by measuring the change in UV–vis absorbance. Under a neutral or acidic condition, 4-NP solution was light yellow in color and exhibited a strong absorption peak at ~307 nm (Fig. 7(a)). Upon the addition of $NaBH_4$, the alkalinity of the solution increased and p-nitrophenolate anions became the dominated species,

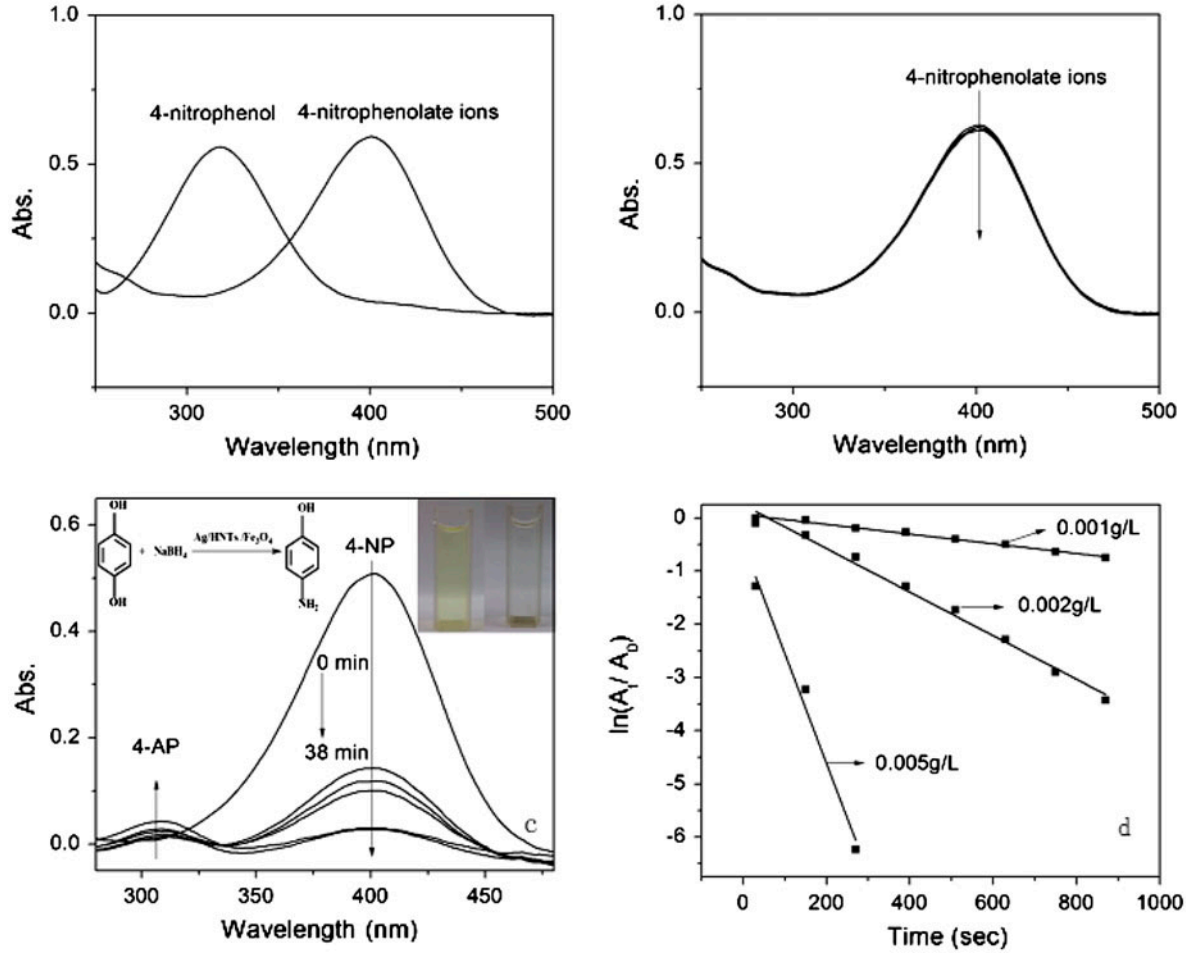

Fig. 7. UV–vis spectra of 4-NP before and after addition of $NaBH_4$ solution (a), 4-NP with $NaBH_4$ without addition of catalysts (b), 4-NP with $NaBH_4$ in the presence of $Ag/HNTs/Fe_3O_4$ as catalysts (c), and the inset is a photograph of the reduction of 4-NP by $NaBH_4$ in the absence and presence of $Ag/HNTs/Fe_3O_4$, Plots of ln (A_t/A_0) vs. time for the reduction of 4-NP by $NaBH_4$ in the presence of different concentration of $Ag/HNTs/Fe_3O_4$ (d).

together with a spectral shift to 400 nm for the absorption peak due to the formation of 4-nitrophenolate. Without the addition of catalyst, the reduction cannot proceed and the maximum absorption peak remained unaltered over time. Thus, the mixture maintained a yellow color which was indicated that it was difficult to proceed without a catalyst (Fig. 7(b)). However, when a trace amount of as-prepared catalyst was introduced into the reaction solution, reduction of 4-NP proceeded rapidly as can be seen from the bleaching of the yellow color over 38 min, indicating complete conversion of 4-NP [48]. Compared with the study results of Lin et al. [49], the as-prepared catalyst also exhibited high catalytic activity. Time-dependent UV–visible absorption spectra (Fig. 7(c)) showed the absorption peak at 400 nm gradually decreased in intensity as the reduction reaction proceeded, while the absorption at 300 nm increased gradually, suggesting the successful reduction of 4-NP and facile formation of 4-AP [50,51], respectively. These results suggested that $Ag/HNTs/Fe_3O_4$ nanoparticles were effective catalysts for similar reactions.

In our reaction system, the concentration of BH_4^- was very high compared with those of 4-NP and catalyst, which can be assumed to be essentially constant during the reaction and this high concentration protects the 4-AP from aerial oxidation [52]. Fig. 7(d) showed that after the induction time there was a good linear relation between ln (A_t/A_0) and time t for all samples, indicating that the reaction followed pseudo-first-order kinetics. The pseudo-first-order kinetics with respect to 4-NP can be applied to evaluate the

Table 2
Details of the catalytic study done for different concentrations of Ag/HNTs/Fe_3O

Sample	Concentration of Ag/HNTs/Fe_3O_4 (g/L)	λ_{max} values of 4-NP at different time intervals		Calculated rate constant ($10^{-3}\,s^{-1}$)	Approximate time completion of reaction
		0.5 min	1.5 min		
1	0.001	0.503	0.491	0.40	38 min
2	0.002	0.450	0.352	4.12	10 min
3	0.005	0.141	0.042	20.18	2.0 min

catalytic rate. The rate constant (k) was determined by a linear plot of ln (C_t/C_0) vs. reduction time. The ratio of C_t to C_0, where C_t and C_0 were the concentrations of 4-NP at time t and 0, respectively, was measured from the relative intensity of the respective absorbance, A_t/A_0 [53]. The catalytic activity of Ag/HNTs/Fe_3O_4 obtained from three different concentrations were also studied (Table 2). The Ag/HNTs/Fe_3O_4 concentration was varied, while other parameters were kept constant for three catalytic runs. It was clear that when $0.001\,g\,L^{-1}$ Ag/HNTs/Fe_3O_4 was added, k was $0.40 \times 10^{-3}\,s^{-1}$ and the time of completion of reaction was approximate 38 min. When $0.002\,g\,L^{-1}$ concentration of catalyst was used, the rate constant ($k = 4.12 \times 10^{-3}\,s^{-1}$) was higher and the reaction finished in a shorter time (10 min). Moreover, the rate constant ($k = 20.18 \times 10^{-3}\,s^{-1}$) was reached to the highest and the reaction time rapidly reduced to 2.0 min when $0.005\,g\,L^{-1}$ catalyst was used. From the result mentioned above, it is clear that k increased with an increase in Ag/HNTs/Fe_3O_4 concentration due to the increase in the number of reaction sites.

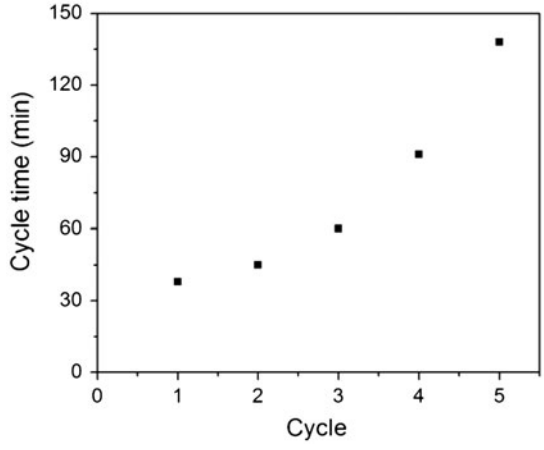

Fig. 8. Time required for total conversion of 4-NP in each catalytic cycle.

3.7. Recycling

To demonstrate magnetic recovery of the assemblies, the catalysts were quickly separated from the solution using an external magnetic field, rinsed several times with deionized water, and dispersed into deionized water for the next cycle of catalysis. As shown in Fig. 8, the catalyst presented favorable in recoverability and reusability, all with conversions of 100% for 4-NP within 60 min in the first three cycles. However, the time required to reach complete reduction is longer, increasing with the number of cycles after three cycles. This fact could be probably due to gradual loss of the catalyst by washing during the repeated magnetic separation.

4. Conclusions

In summary, we have demonstrated the fabrication of recoverable supports HNTs/Fe_3O_4, then HNTs/Fe_3O_4 nanoparticles deposited with highly dispersed Ag particles were obtained in high yield in $Ag(NH_3)_2^+$ solutions with the aid of glucoses reducer. The catalyst was characterized by UV–visible spectroscopy, XRD, SEM, TEM, EDS, FT-IR, TG, and magnetization curves analysis which illustrated that Fe_3O_4 in internal tube and Ag particles in external surface were observed to be spherical in shape with a mean diameter of 7.0 and 30 nm, respectively. The effectiveness of the as-prepared Ag/HNTs/Fe_3O_4 as catalyst for 4-NP reduction to 4-AP by excess borohydride was evaluated and the 4-NP could be reduced thoroughly in 38 min. It turned out that this type of compound was promising to provide a reaction-selective catalyst. Furthermore, the influence of different concentrations of catalyst was also discussed and the rate constant increased with an increase in Ag/HNTs/Fe_3O_4 concentration. The new as-prepared catalysts are stable, efficient, eco-friendly, easy to prepare, and recyclable and thus have potential for industrial applications.

Acknowledgments

This work was financially supported by the National Natural Science Foundation of China (Nos. 21107037, 21176107), Natural Science Foundation of Jiangsu Province (Nos. BK2011461, BK2011514), National Postdoctoral Science Foundation (No. 2013M530240), Postdoctoral Science Foundation funded Project of Jiangsu Province (No. 1202002B) and Programs of Senior Talent Foundation of Jiangsu University (No. 12JDG090).

References

[1] T.C. Wang, N. Lu, J. Li, Y. Wu, Plasma-TiO_2 catalytic method for high-efficiency remediation of p-nitrophenol contaminated soil in pulsed discharge, Environ. Sci. Technol. 45 (2011) 9301–9307.

[2] A. Chauhan, G. Pandey, N.K. Sharma, D. Paul, J. Pandey, R.K. Jain, p-Nitrophenol degradation via 4-nitrocatechol in *Burkholderia* sp. SJ98 and cloning of some of the lower pathway genes, Environ. Sci. Technol. 44 (2010) 3435–3441.

[3] S. Labana, G. Pandey, D. Paul, N.K. Sharma, A. Basu, R.K. Jain, Pot and field studies on bioremediation of p-nitrophenol contaminated soil using arthrobacter protophormiae RKJ100, Environ. Sci. Technol. 39 (2005) 3330–3337.

[4] M. Shimazu, A. Mulchandani, W. Chen, Simultaneous degradation of organophosphorus pesticides and p-nitrophenol by a genetically engineered *Moraxella* sp. with surface-expressed organophosphorus hydrolase, Biotechnol. Bioeng. 76 (2001) 318–324.

[5] A. Schackmann, R. Muller, Reduction of nitroaromatic compounds by different Pseudomonas species under aerobic conditions, Appl. Microbiol. Biotechnol. 34 (1991) 809–813.

[6] T.O. Stevens, R.L. Crawford, D.L. Crawford, Selection and isolation of bacteria capable of degrading dinoseb (2-s-butyl-4,6-dinitrophenol), Biodegradation 2 (1991) 1–13.

[7] M. Ahmaruzzaman, S.L. Gayatri, Activated tea waste as a potential low-cost adsorbent for the removal of p-nitrophenol from wastewater, Chem. Eng. 55 (2010) 4614–4623.

[8] S.S. Zhang, J.M. Song, H.L. Niu, C.J. Mao, S.Y. Zhang, Y.H. Shen, Facile synthesis of antimony selenide with lamellar nanostructures and their efficient catalysis for the hydrogenation of p-nitrophenol, J. Alloys Compd. 585 (2014) 40–47.

[9] J.M. Song, S.S. Zhang, Sh.H. Yu, Multifunctional $Co_{0.85}Se$–Fe_3O_4 nanocomposites: Controlled synthesis and their enhanced performances for efficient hydrogenation of *p*-Nitrophenol and adsorbents, Small 10 (2014) 717–724.

[10] Z.H. Bai, R. Chen, P. Si, Y.J. Huang, H.D. Sun, D.H. Kim, Fluorescent pH sensor based on Ag@SiO_2 core-shell nanoparticle, ACS Appl. Mater. Interfaces 5 (2013) 5856–5860.

[11] R. Eising, A.M. Signori, S. Fort, J.B. Domingos, Development of catalytically active silver colloid nanoparticles stabilized by dextran, Langmuir 27 (2011) 11860–11866.

[12] K.H. Kim, Y.B. Lee, S.G. Lee, H.C. Park, S.S. Park, Preparation of fine nickel powders in aqueous solution under wet chemical process, Mat. Sci. Eng. A 381 (2004) 337–342.

[13] X. Ni, J. Zhang, Y. Zhang, H. Zheng, Citrate-assisted synthesis of prickly nickel microwires and their surface modification with silver, J. Colloid Interface Sci. 307 (2007) 554–558.

[14] M.L. Singla, A. Negi, V. Mahajan, K.C. Singh, D.V.S. Jain, Catalytic behavior of nickel nanoparticles stabilized by lower alkylammonium bromide in aqueous medium, Appl. Catal., A 323 (2007) 51–57.

[15] D.E. Zhang, X.M. Ni, H.G. Zheng, Y. Li, X.J. Zhang, Z.P. Yang, Synthesis of needle-like nickel nanoparticles in water-in-oil microemulsion, Mater. Lett. 59 (2005) 2011–2014.

[16] D.H. Chen, S.H. Wu, Synthesis of nickel nanoparticles in water-in-oil microemulsions, Chem. Mater. 12 (2000) 1354–1360.

[17] Z.F. Jiang, J.M. Xie, D.L. Jiang, X.J. Wei, M. Chen, Modifiers-assisted formation of nickel nanoparticles and their catalytic application to p-nitrophenol reduction, Cryst. Eng. Comm. 15 (2012) 560–569.

[18] S.J. Li, S.Q. Gong, A positively temperature-responsive, substrate-sective Ag nanoreactor, J. Phys. Chem. B 113 (2009) 16501–16507.

[19] Y. Lu, Y. Mei, M. Schrinner, M. Ballauff, M.W. Moller, J. Breu, In situ formation of Ag nanoparticles in spherical polyacrylic acid brushes by UV irradiation, J. Phys. Chem. C 111 (2007) 7676–7681.

[20] H. Yu, Y. Zhang, J. Zhang, H. Zhang, J. Liu, Preparation and antibacterial property of SiO_2-Ag/PES hybrid ultrafiltration membranes, Desalin. Water Treat. 51 (2013) 3584–3590.

[21] Z. Deng, M. Chen, L. Wu, Novel method to fabricate SiO_2/Ag composite spheres and their catalytic, surface-enhanced raman scattering properties, J. Phys. Chem. C 111 (2007) 11692–11698.

[22] L. Yang, W. Luo, G.Z. Cheng, Graphene-support Ag-based core-shell nanoparticles for hydrogen generation in hydrolysis of ammonia borane and methylamine borane, Appl. Mater. Interfaces 5 (2013) 8231–8240.

[23] Y.C. Chen, R.J. Young, J.V. Macpherson, N.R. Wilson, Single-walled carbon nanotube networks decorated with silver nanoparticles: A novel graded SERS substrate, J. Phys. Chem. C 111 (2007) 16167–16173.

[24] R.X. Dong, C.T. Liu, K.C. Huang, W.Y. Chiu, K.C. Ho, J.J. Lin, Controlling formation of silver/carbon nanotube networks for highly conductive film surface, ACS Appl. Mater. Interfaces 4 (2012) 1449–1455.

[25] J.Y. Zhang, Y.T. Zhang, Y.Y. Chen, L. Du, B. Zhang, H.Q. Zhang, J.D. Liu, K.J. Wang, Preparation and characterization of novel polyethersulfone hybrid ultrafiltration membranes bending with modified halloysite nanotubes loaded with silver nanoparticles, Ind. Eng. Chem. Res. 51 (2012) 3081–3090.

[26] J.M. Pan, H. Yao, L.C. Xu, H.X. Ou, P.W. Huo, X.X. Li, Y.S. Yan, Selective recognition of 2,4,6-trichlorophenol by molecularly imprinted polymers based on magnetic halloysite nanotubes composites, J. Phys. Chem. C 115 (2011) 5440–5449.

[27] D.G. Shchukin, S.V. Lamaka, K.A. Yasakau, M.L. Zheludkevich, M.G.S. Ferreira, H. Mohwald, Active

anticorrosion coatings with halloysite nanocontainers, J. Phys. Chem. C 112 (2008) 958–964.
[28] G. Kiani, M. Dostali, A.R. Khataee, Adsorption studies on the removal of Malachite Green from aqueous solutions onto halloysite nanotubes, Appl. Clay Sci. 54 (2011) 34–39.
[29] S.B. Barrientos-Ramírez, G.M.O. Oca-Ramírez, E.V.R. Ramos-Fernández, A. Sepúlveda-Escribano, M.M. Pastor-Blas, A. González-Montiel, Surface modification of natural halloysite clay nanotubes with aminosilanes. Application as catalyst supports in the atom transfer radical polymerization of methyl methacrylate, Appl. Catal., A 406 (2011) 22–33.
[30] R. Zhai, B. Zhang, Y.Z. Wan, C.C. Li, J.T. Wang, J.D. Liu, Chitosan–halloysite hybrid-nanotubes: Horseradish peroxidase immobilization and applications in phenol removal, Chem. Eng. J. 214 (2013) 304–309.
[31] S.J. Ding, Y.C. Xing, M. Radosz, Y.Q. Shen, Magnetic nanoparticle supported catalyst for atom transfer radical polymerization, Macromolecules 39 (2006) 6399–6405.
[32] H.C. Dong, J.Y. Huang, R.E. Koepsel, P.L. Ye, A.J. Russell, K. Matyjaszewski, Recyclable antibacterial magnetic nanoparticles grafted with quaternized poly (2-(dimethylamino)ethyl methacrylate) brushes, Biomacromolecules 12 (2011) 1305–1311.
[33] Y.H. Zhu, J.H. Shen, K.F. Zhou, C. Chen, X.L. Yang, C.Z. Li, Multifunctional magnetic composite microspheres with *in situ* growth Au nanoparticles: A highly efficient catalyst system, J. Phys. Chem. C 115 (2011) 1614–1619.
[34] H. Hui, C.X. Li, J.M. Pan, L.Z. Li, J.D. Dai, X.H. Dai, P. Yu, Y.H. Feng, Selective separation of lambdacyhalothrin by porous/magnetic molecularly imprinted polymers prepared by Pickering emulsion polymerization, J. Sep. Sci. 36 (2013) 3285–3294.
[35] L.T. Qu, L.M. Dai, Novel silver nanostructures from silver mirror reaction on reactive substrates, J. Phys. Chem. B 109 (2005) 13985–13990.
[36] D.B. Yu, V.W.W. Yam, Hydrothermal-induced assembly of colloidal silver spheres into various nanoparticles on the basis of HTAB-modified silver mirror reaction, J. Phys. Chem. B 109 (2005) 5497–5503.
[37] J. Zeng, Q. Zhang, J.Y. Chen, Y.N. Xia, A comparison study of the catalytic properties of Au-based nanocages, nanoboxes, and nanoparticles, Nano Lett. 10 (2010) 30–35.
[38] Z.H. Bai, R. Chen, P. Si, Y.J. Huang, H.D. Sun, D.H. Kim, Fluorescent pH sensor based on Ag@SiO_2 core-shell nanoparticle, ACS Appl. Mater. Interfaces 5 (2013) 5856–5860.
[39] R.J. Wang, G.H. Jiang, Y.W. Ding, Y. Wang, X.K. Sun, X.H. Wang, W.X. Chen, Photocatalytic activity of heterostructures based on TiO_2 and halloysite nanotubes, ACS Appl. Mater. Interfaces 3 (2011) 4154–4158.
[40] C.H. Liu, Z.D. Zhou, X. Yu, B.Q. Lv, J.F. Mao, D. Xiao, Prepartion and characterrization of Fe_3O_4/Ag composite magnetic nanoparticles, Inorg. Mater. 44 (2008) 291–295.
[41] K.H. Chen, Y.C. Pu, K.D. Chang, Y.F. Liang, C.M. Liu, J.W. Yeh, H.C. Shih, Y.J. Hsu, Ag-nanoparticle-decorated SiO_2 nanospheres exhibiting remarkable plasmon-mediated photocatalytic properties, J. Phys. Chem. C 116 (2012) 19039–19045.
[42] X. Zhang, Z.H. Su, Polyelectrolyte-multilayer-supported Au@Ag core-shell nanoparticles with high catalytic activity, Adv. Mater. 24 (2012) 4574–4577.
[43] Y. Lin, K.M. Ng, C.M. Chan, G.X. Sun, J.S. Wu, High-impact polystyrene/halloysite nanocomposites prepared by emulsion polymerization using sodium dodecyl sulfate as surfactant, J. Colloid Interface Sci. 358 (2011) 423–429.
[44] S. Pal, G. De, A new approach for the synthesis of Au–Ag alloy nanoparticle incorporated SiO_2 films, Chem. Mater. 17 (2005) 6161–6166.
[45] X.L. Tang, W. Qian, A. Hu, Y.M. Zhao, N.N. Fei, L. Shi, Adsorption of thiophene on Pt/Ag-supported activated carbons prepared by ultrasonic-assisted impregnation, Ind. Eng. Chem. Res. 50 (2011) 9363–9367.
[46] D. Tan, P. Yuan, F. Annabi-Bergaya, H. Yu, D. Liu, H. Liu, H. He, Natural halloysite nanotubes as mesoporous carriers for the loading of ibuprofen, Micropor. Mesopor. Mater. 179 (2013) 89–98.
[47] P. Li, A.M. Zhu, Q.L. Liu, Q.G. Zhang, Fe_3O_4/poly(N-isopropylacrylamide)/chitosan composite microspheres with multiresponsive properties, Ind. Eng. Chem. Res. 47 (2008) 7700–7706.
[48] J.P. Ge, T. Huynh, Y.X. Hu, Y.D. Yin, Hierarchical magnetite/silica nanoassemblies as magnetically recoverable catalyst-supports, Nano Lett. 8 (2008) 931–934.
[49] L. Lin, K. Shang, X.T. Xu, C.X. Chu, H.H. Ma, Y.I. Lee, J.C. Hao, H.G. Liu, Formation of Ag nanoparticle-doped foam-like polymer films at the liquid–liquid interface, J. Phys. Chem. B 115 (2011) 11113–11118.
[50] K. Hayakawa, T. Yoshimura, K. Esumi, Preparation of gold–dendrimer nanocomposites by laser irradiation and their catalytic reduction of 4-Nitrophenol, Langmuir 19 (2003) 5517–5521.
[51] S. Praharaj, S. Nath, S.K. Ghosh, S. Kundu, T. Pal, Immobilization and recovery of Au nanoparticles from anion exchange resin: resin-bound nanoparticle matrix as a catalyst for the reduction of 4-nitrophenol, Langmuir 20 (2005) 9889–9892.
[52] J.F. Huang, S. Vongehr, S.C. Tang, H.M. Lu, J.C. Shen, X.K. Meng, Ag dendrite-based Au/Ag bimetallic nanostructures with strongly enhanced catalytic activity, Langmuir 25 (2009) 11890–11896.
[53] Q. An, M. Yu, Y.T. Zhang, W.F. Ma, J. Guo, C.C. Wang, Fe_3O_4@Carbon microsphere supported Ag–Au bimetallic nanocrystals with the enhanced catalytic activity and selectivity for the reduction of nitroaromatic compounds, J. Phys. Chem. C 116 (2012) 22432–22440.